

---

---

# Comparative Dosimetry for $^{68}\text{Ga}$ -DOTATATE: Impact of Using Updated ICRP Phantoms, S Values, and Tissue-Weighting Factors

Anders Josefsson<sup>1</sup>, Robert F. Hobbs<sup>1,2</sup>, Sagar Ranka<sup>1</sup>, Bryan C. Schwarz<sup>3</sup>, Donika Plyku<sup>1</sup>, Jose Willegaignon de Amorim de Carvalho<sup>4</sup>, Carlos Alberto Buchpiguel<sup>4</sup>, Marcelo Tatit Sapienza<sup>4</sup>, Wesley E. Bolch<sup>3</sup>, and George Sgouros<sup>1</sup>

<sup>1</sup>Russell H. Morgan Department of Radiology and Radiological Science, School of Medicine, Johns Hopkins University, Baltimore Maryland; <sup>2</sup>Department of Radiation Oncology, School of Medicine, Johns Hopkins University, Baltimore Maryland; <sup>3</sup>Department of Biomedical Engineering, University of Florida, Gainesville, Florida; and <sup>4</sup>Instituto do Cancer do Estado de São Paulo, School of Medicine, São Paulo University, São Paulo, Brazil

The data that have been used in almost all calculations of MIRD S value absorbed dose and effective dose are based on stylized anatomic computational phantoms and tissue-weighting factors adopted by the International Commission on Radiological Protection (ICRP) in its publication 60. The more anatomically realistic phantoms that have recently become available are likely to provide more accurate effective doses for diagnostic agents.  $^{68}\text{Ga}$ -DOTATATE is a radiolabeled somatostatin analog that binds with high affinity to somatostatin receptors, which are overexpressed in neuroendocrine tumors and can be used for diagnostic PET/CT-based imaging. Several studies have reported effective doses for  $^{68}\text{Ga}$ -DOTATATE using the stylized Cristy–Eckerman (CE) phantoms from 1987; here, we present effective dose calculations using both the ICRP 60 and more updated formalisms. **Methods:** Whole-body PET/CT scans were acquired for 16 patients after  $^{68}\text{Ga}$ -DOTATATE administration. Contours were drawn on the CT images for spleen, liver, kidneys, adrenal glands, brain, heart, lungs, thyroid gland, salivary glands, testes, red marrow (L1–L5), muscle (right thigh), and whole body. Dosimetric calculations were based on the CE phantoms and the more recent ICRP 110 reference-voxel phantoms. Tissue-weighting factors from ICRP 60 and ICRP 103 were used in effective dose calculations for the CE phantoms and ICRP 110 phantoms, respectively. **Results:** The highest absorbed dose coefficients (absorbed dose per unit activity) were, in descending order, in the spleen, pituitary gland, kidneys, adrenal glands, and liver. For ICRP 110 phantoms with tissue-weighting factors from ICRP 103, the effective dose coefficient was  $0.023 \pm 0.003$  mSv/MBq, which was significantly lower than the  $0.027 \pm 0.005$  mSv/MBq calculated for CE phantoms with tissue-weighting factors from ICRP 60. One of the largest differences in estimated absorbed dose coefficients was for the urinary bladder wall, at  $0.040 \pm 0.011$  mGy/MBq for ICRP 110 phantoms compared with  $0.090 \pm 0.032$  mGy/MBq for CE phantoms. **Conclusion:** This study showed that the effective dose coefficient was slightly overestimated for CE phantoms, compared with ICRP 110 phantoms using the latest tissue-weighting factors from ICRP 103. The more detailed handling of electron transport in the latest phantom calculations gives significant differences in estimates of the absorbed dose to stem cells in the walled organs of the alimentary tract.

**Key Words:**  $^{68}\text{Ga}$ -DOTATATE; PET/CT imaging; normal tissue; dosimetry; effective dose

**J Nucl Med 2018; 59:1281–1288**

DOI: 10.2967/jnumed.117.203893

**D**osimetry for nuclear medicine imaging agents is performed to ensure that the long-term radiation risks of the imaging procedure are minimal compared with the benefits of obtaining a correct image-based diagnosis. In the late 1960s and early 1970s, the MIRD Committee of the Society of Nuclear Medicine and Molecular Imaging published a formalism that standardized the process for computing tissue-absorbed doses through the introduction of 2 essential terms, *cumulated activity* ( $\tilde{A}$ ) and *radionuclide S value* (S) (1). Cumulated activity, currently known by the term *time-integrated activity* (abbreviated TIA but still represented by  $\tilde{A}$ ) (2), depends on the pharmacokinetic properties of the diagnostic agent. These are typically characterized by longitudinal quantitative imaging in an appropriate patient population. S value is defined as the absorbed dose to a target region per unit TIA in the source region, such that the product of TIA and S value gives the absorbed dose contribution from a source region to a target region. S values depend on the emission characteristics of the radionuclide used in the diagnostic agent and on the reference anatomic model used in the Monte Carlo radiation transport simulations of the emitted radiation particles and photons. The S values that have been used in effective dose calculations over the past several decades have been derived primarily from the stylized Cristy–Eckerman (CE) phantom series developed in 1987 (3) and used extensively by the International Commission on Radiological Protection (ICRP). Reflecting the computational and imaging capabilities of the time, the CE phantoms comprised stylized organs composed of simple geometries defined by mathematic surface equations to describe the inner anatomy and outer body contour. In 2009, the ICRP and the International Commission on Radiation Units and Measurements released adult male and female CT-based voxelized reference phantoms (ICRP publication 110) (4), with organ and tissue masses matched to reference values (ICRP publication 89) (5). Specific absorbed fractions for the ICRP 110 voxelized reference phantoms have been published (ICRP publication 133) (6), as well as the latest reference tissue-weighting factors (ICRP publication 103) (7).

Received Oct. 18, 2017; revision accepted Dec. 14, 2017.

For correspondence or reprints contact: George Sgouros, Russell H. Morgan Department of Radiology and Radiological Science, Johns Hopkins University, School of Medicine, CRBII 4M.61, 1550 Orleans St., Baltimore, MD 21231.

E-mail: gsgouros@jhmi.edu

Published online Feb. 9, 2018.

COPYRIGHT © 2018 by the Society of Nuclear Medicine and Molecular Imaging.

In the present study, we used  $^{68}\text{Ga}$ -DOTATATE PET/CT scans to compare dosimetry based on the most recent ICRP standards (ICRP 110 phantoms and ICRP 103 tissue-weighting factors) with dosimetry based on the prior standards (CE phantoms and ICRP 60 tissue-weighting factors (8)) and with previously reported dosimetry based on these prior standards (9,10). Such comparisons are important to understanding the impact of transitioning from the older phantoms and tissue-weighting factors to the most recently recommended ones.

## MATERIALS AND METHODS

### Patients

$^{68}\text{Ga}$ -DOTATATE PET/CT scans from 16 Brazilian patients with somatostatin-avid tumors were used in this study (11 female and 5 male; mean age,  $53.8 \pm 13.0$  y; range, 36–79 y) (Table 1). PET was indicated for staging, follow-up, or planning of peptide receptor radionuclide therapy. Five of the patients had gastroenteropancreatic neuroendocrine tumors, 5 had medullary thyroid cancer with increasing calcitonin levels, 3 had neuroectodermic tumors (malignant pheochromocytoma or paraganglioma), 2 had associated adrenal and thyroid tumors, and 1 had ectopic Cushing syndrome requiring tumor localization. The institutional review board at São Paulo University School of Medicine approved this study, and all subjects signed an informed-consent form.

### PET/CT Imaging

Two to four whole-body PET/CT scans were acquired at 2–240 min after injection of  $^{68}\text{Ga}$ -DOTATATE (mean,  $131.2 \pm 26.3$  MBq) (Table 1). Imaging was performed in 3-dimensional time-of-flight mode on a Discovery PET/CT 690 system (GE Healthcare) at 2 min per bed position. The acquisition matrix was  $192 \times 192$  pixels, the in-slice pixel size was 3.27 mm, and the transaxial slice thickness was 3.27 mm. Ordered-subsets expectation maximization was used for PET reconstruction, with CT-based attenuation correction using automatic exposure control for dose reduction.

### Normal-Tissue Dosimetry

*Overview.* Patient-tissue activity concentrations rather than organ-specific activities were taken from the patient data and transposed into

**TABLE 1**  
Patient and Imaging Data

Patient	Age (y)	Weight (kg)	Height (cm)	Sex	Administered activity (MBq)	PET/CT scans (n)
1F	59	63	155	F	156.9	3
2F	67	75	145	F	107.3	3
3F	70	74	147	F	140.6	4
4F	53	66	165	F	126.2	2
5F	35	76	161	F	107.3	3
6F	38	62	167	F	125.8	2
7F	65	109	159	F	82.1	3
8M	36	83	178	M	149.1	2
9F	79	73	156	F	177.6	3
10M	59	68	157	M	169.5	3
11M	63	102	182	M	158.7	3
12M	39	85	181	M	91.0	3
13F	43	97	155	F	112.1	2
14M	44	94	176	M	137.3	2
15F	52	106	162	F	126.5	3
16F	58	84	157	F	131.7	3

the 2 reference phantom models. Normal-tissue absorbed dose coefficients (absorbed dose per unit activity) were calculated using the MIRD S-value-based methodology (1,2). OLINDA/EXM software, version 1 (11), was used for the CE phantom dosimetry calculations, and a Microsoft Excel spreadsheet with S values obtained from the University of Florida was used for the ICRP 110 phantom dosimetry calculations. TIA (i.e., total number of nuclear transformations between 2 time points) was calculated from time-activity data within the source regions, defined by drawing organ contours on the CT portion of the first PET/CT image for each patient. These contours were transposed to later time points after deformable registration of the scans had been performed using Velocity software (version 3.1; Varian Medical Systems Inc.). Contours were drawn for the spleen, liver, kidneys, adrenal glands, brain, heart, lungs, thyroid gland, salivary glands, testes, red marrow (L1–L5), muscle (right thigh), and whole body. Dosimetry was performed for each patient and inserted into the respective phantom, after which the average for all patients was calculated.

*TIA Calculations.* The average activity concentration is  $\frac{A(r_S, t)}{V(r_S)}$ , where  $A$  is activity,  $V$  is volume,  $r_S$  is source region, and  $t$  is time after injection. Volume was derived from each patient's PET/CT images. The specific organ/tissue activity (Bq) for a phantom  $\kappa$  was calculated for each patient's organ/tissue activity as follows:

$$A(r_S, t)_\kappa = \frac{A(r_S, t)}{V(r_S)} \cdot \frac{M(r_S)_\kappa}{\rho(r_S)}, \quad \text{Eq. 1}$$

where  $M$  is mass and  $\rho$  is tissue density. Mass was taken from OLINDA/EXM (11,12) for the CE phantom calculations and from ICRP 133 for the ICRP 110 phantom calculations. Tissue density was according to ICRP 110. Source region  $r_S$  in Equation 1 is an index over all tissues and the whole body for which TIA was assigned.

Excel was used to fit a monoexponential expression to each patient's specific organ/tissue time-activity curve. The expressions were analytically integrated from 0 to infinity, resulting in the TIA corresponding to each phantom's source region. Preserving activity concentration rather than total activity can lead to a discrepancy in the whole-body activity between the phantom and the patient at the time of administration. The TIA coefficient (TIAC) is defined as the TIA divided by the administered activity. In this scenario, the administered activity is the total virtually administered activity to the phantom rather than the administered activity to the patient. Scaling of each TIAC by the phantom-to-patient whole-body mass ratio accounts for this difference. The TIAs (Bq-s) used for the calculations were as follows:

$$\tilde{A}(r_S)_\kappa = \int_0^\infty A(r_S, t)_\kappa dt. \quad \text{Eq. 2}$$

The TIACs (s) where

$$\tilde{a}(r_S)_\kappa = \frac{M(wb)_{patient}}{M(wb)_\kappa} \cdot \frac{\tilde{A}(r_S)_\kappa}{A_0}, \quad \text{Eq. 3}$$

where  $\tilde{a}$  is TIAC,  $wb$  is whole body, and  $A_0$  is administered activity.

*Remainder of Body.* The remainder-of-body TIAC (s) was calculated as the difference between the TIAC of the whole body, the TIAC of the target region, and the TIAC of the source regions summed:

$$\tilde{a}(rb)_\kappa = \tilde{a}(wb)_\kappa - \tilde{a}(r_T)_\kappa - \sum_{r_S} \tilde{a}(r_S)_\kappa, \quad \text{Eq. 4}$$

where  $rb$  is rest of body,  $wb$  is whole body, and  $r_T$  is target region. The corresponding phantom masses (kg) were

$$M(rb)_\kappa = M(wb)_\kappa - M(r_T)_\kappa - \sum_{r_S} M(r_S)_\kappa, \quad \text{Eq. 5}$$

Source region  $r_S$  in Equations 4 and 5 is an index over all source regions for which a TIAC is assigned, except for the target region. The remainder-of-body mass excluded the contents of the walled organs.

*Urinary Bladder.* The TIAC for urinary bladder contents was calculated using the MIRD bladder-voiding model (13) as implemented in OLINDA/EXM. A 2-h voiding interval was used, with the whole-body biologic clearance half-life obtained from the PET/CT images and a fraction of 1. This TIAC was used both for the CE phantom calculations and for the ICRP 110 phantom calculations.

*Pituitary Gland.* To account for partial-volume effects arising from the small size of the pituitary gland, a hybrid dosimetric method developed by Plyku et al. (14) for small tumors was used. Briefly, the pituitary gland was modeled as a 0.6-g unit-density sphere. A 10% threshold of the maximum PET value was used for contouring. The volume of the pituitary gland contoured on the PET images was systematically larger than the ICRP volume and presumably larger than the real volume because of activity spill-out. However, this volume contains the activity in the pituitary gland plus some background activity (Bq) in the PET volume outside the real volume, which needs to be subtracted:

$$A(\text{pg}) = A(V_{\text{PET}}) - \frac{A}{V}(\text{bkg}) \cdot (V_{\text{PET}} - V_{\text{ICRP}}), \quad \text{Eq. 6}$$

where pg is pituitary gland and bkg is background. The background activity concentration for the pituitary gland was determined by drawing a contour in the brain. A monoexponential expression was fitted to the time-activity data points and analytically integrated from zero to infinity, and the TIAC was calculated according to Equations 2 and 3 for the respective phantom.

*Absorbed Dose Calculations.* The MIRD Committee-derived equation was used for all calculations of absorbed dose coefficients (absorbed dose per unit activity (Gy/Bq)) (2):

$$d(r_T) = \sum_{r_S} \tilde{a}(r_S) \cdot S(r_T \leftarrow r_S), \quad \text{Eq. 7}$$

where  $d$  is absorbed dose coefficient. The TIACs for the CE phantoms were used as input in OLINDA/EXM to obtain estimates of the CE phantom-derived absorbed dose coefficient. Because the CE phantoms do not have S values for the pituitary gland, the self-dose absorbed dose coefficient to the pituitary gland was calculated using the unit-density sphere model provided by OLINDA/EXM. An Excel spreadsheet was used for the ICRP dosimetric calculations.

*Remainder-of-Body Contribution to Absorbed Dose.* The CE phantom-based dosimetry specifies 25 target regions and 28 source regions. In contrast, the ICRP 110 phantom dosimetry allows TIAC apportionment in up to 76 source regions and provides the absorbed dose coefficients to 41 target regions. More significantly, the CE phantom-based formalism includes whole-body-to-individual-tissue S values, whereas no such S values are tabulated for the ICRP 110 phantoms. The remainder TIAC that has not been otherwise allocated is given the term *remainder of body* in CE phantom calculations. Target absorbed dose coefficients (Gy/Bq) for remainder of body are given by (15)

$$d(r_T)_{\text{CE}} = \tilde{a}(r_T)_{\text{CE}} \cdot S(r_T \leftarrow r_T)_{\text{CE}} + \tilde{a}(rb)_{\text{CE}} \cdot S(r_T \leftarrow rb)_{\text{CE}} + \sum_{r_S} \tilde{a}(r_S)_{\text{CE}} \cdot S(r_T \leftarrow r_S)_{\text{CE}}, \quad \text{Eq. 8}$$

with the remainder-of-body to target S value (Gy/Bq-s) given by

$$S(r_T \leftarrow rb)_{\text{CE}} = S(r_T \leftarrow wb)_{\text{CE}} \cdot \frac{M(wb)_{\text{CE}}}{M(rb)_{\text{CE}}} - \sum_{r_S} S(r_T \leftarrow r_S)_{\text{CE}} \cdot \frac{M(r_S)_{\text{CE}}}{M(rb)_{\text{CE}}}. \quad \text{Eq. 9}$$

Because almost all tissues in the body are accounted for by the ICRP 110 phantoms, whole-body-to-individual-tissue S values have not been calculated for the ICRP 110 phantoms. The contribution of the absorbed dose coefficient from remainder of body to each target tissue is obtained by apportioning the remainder-of-body TIAC (s) to each remaining source tissue not previously accounted for:

$$\tilde{a}(r_U)_{\text{ICRP}} = \tilde{a}(rb)_{\text{ICRP}} \cdot \frac{M(r_U)_{\text{ICRP}}}{M(rb)_{\text{ICRP}}}, \quad \text{Eq. 10}$$

where  $r_U$  is the index over source regions identified in the ICRP 110 phantoms that have not been specifically assigned a TIAC.

The absorbed dose coefficient (Gy/Bq) to each target region of the ICRP 110 phantoms is given by

$$d(r_T)_{\text{ICRP}} = \tilde{a}(r_T)_{\text{ICRP}} \cdot S(r_T \leftarrow r_T)_{\text{ICRP}} + \sum_{r_S} \tilde{a}(r_S)_{\text{ICRP}} \cdot S(r_T \leftarrow r_S)_{\text{ICRP}} + \sum_{r_U} \tilde{a}(r_U)_{\text{ICRP}} \cdot S(r_T \leftarrow r_U)_{\text{ICRP}}. \quad \text{Eq. 11}$$

*Effective Dose Calculations.* The effective dose coefficient (effective dose per unit activity (Sv/Bq)) for CE phantom calculations in an individual patient is given by

$$e_{\text{CE}}^{\text{patient}} = \sum_T w_T \cdot h(r_T)_{\text{CE}}^{\text{patient}}, \quad \text{Eq. 12}$$

where  $e$  is effective dose coefficient,  $w_T$  is ICRP 60 tissue-weighting factor, and  $h$  is equivalent dose coefficient (Sv/Bq).

The radiation-weighting factor for all  $^{68}\text{Ga}$  radiation emissions is equal to 1. Accordingly,

$$h(r_T)_\kappa^\alpha = d(r_T)_\kappa^\alpha, \quad \text{Eq. 13}$$

where  $\alpha$  denotes the sex of each patient.

The effective dose coefficient per unit activity (Sv/Bq) is obtained by averaging the male- and female-averaged patient-specific effective dose coefficient:

$$e_{\text{CE}} = \left[ \frac{\sum_{n_M} e_{\text{CE}}^M + \sum_{n_F} e_{\text{CE}}^F}{2} \right], \quad \text{Eq. 14}$$

where  $n_M$  and  $n_F$  are the number of males and females, respectively.

The effective dose coefficient (Sv/Bq) for ICRP is

$$e_{\text{ICRP}} = \sum_T w_T \cdot \left[ \frac{\sum_{n_M} h(r_T)_{\text{ICRP}}^M + \sum_{n_F} h(r_T)_{\text{ICRP}}^F}{2} \right], \quad \text{Eq. 15}$$

where the tissue-weighting factor is from ICRP 103.

The percentage differences between the CE phantom values and the ICRP 110 phantom values were calculated as follows:

$$\text{Difference} = \frac{(\text{value}_{\text{CE}} - \text{value}_{\text{ICRP}})}{\text{value}_{\text{CE}}} \cdot 100\% \quad \text{Eq. 16}$$

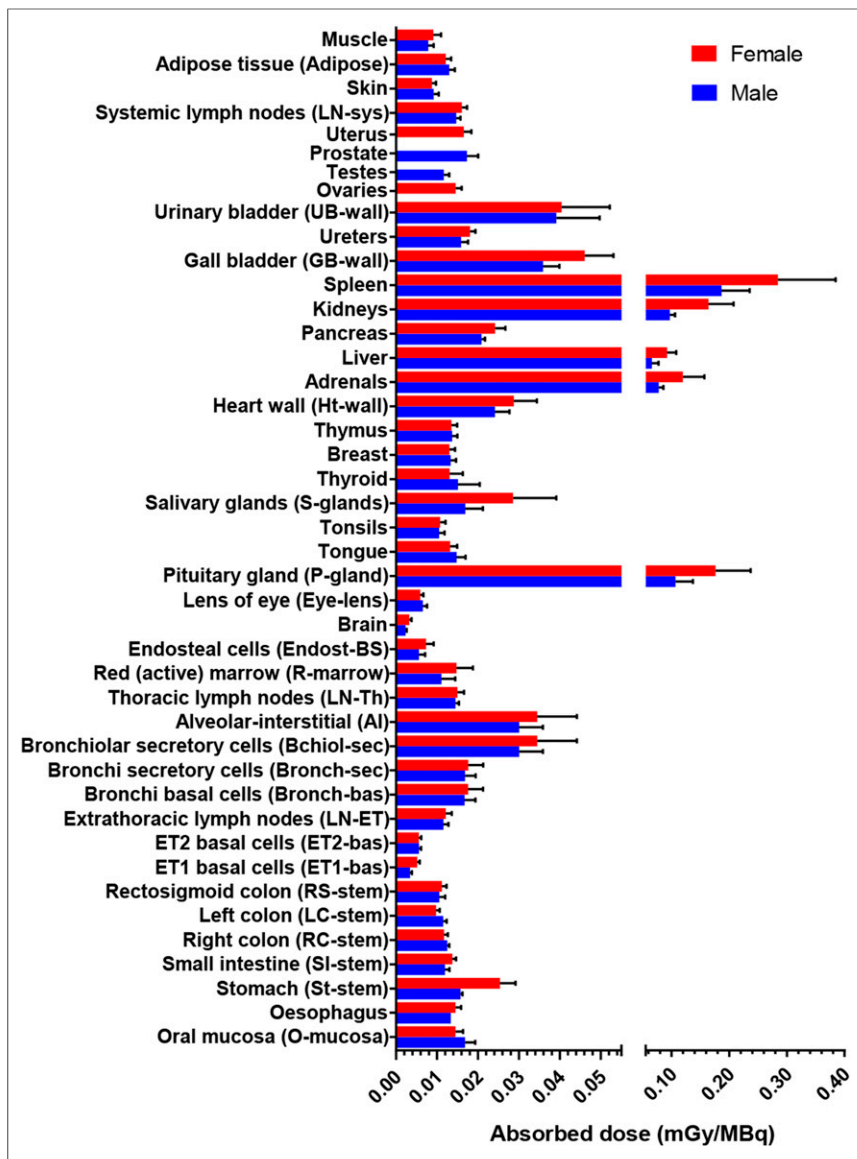


**FIGURE 1.** Mean absorbed dose coefficients for normal organs and tissues using ICRP 110 phantoms. Error bars = SD.

### Statistical Analysis

Statistical analysis was performed using Prism software (version 7.03; GraphPad Software Inc.). All data are presented as the mean value  $\pm$  SD. Groups were compared using a 2-tailed Student *t* test, and differences between groups were considered significant for *P* values of less than 0.05.

### RESULTS

The absorbed dose coefficients calculated for the ICRP 110 phantoms are shown in Figure 1. The tissues with the highest 7 absorbed dose coefficients, as well as the effective dose coefficient, are listed and compared with previously published data (9,10) in Table 2. ICRP 110 phantom-based calculations for the 16 patients are shown in Figure 2. TIACs are listed in Table 3. The absorbed dose coefficients obtained in this study are compared with those in the literature (9) in Figure 3. The ICRP 110 phantom-derived effective dose coefficient ( $0.023 \pm 0.003$  mSv/MBq) obtained using tissue-weighting factors from ICRP 103 was significantly lower ( $P = 0.0114$ ) than that ( $0.027 \pm 0.005$  mSv/MBq) derived from the CE phantoms using tissue-weighting factors from ICRP 60. Significant differences in calculated absorbed dose coefficients between the CE phantoms and the ICRP 110 phantoms were found for gallbladder wall, breast, thymus, pancreas, small intestine wall, stomach wall, uterus, ovaries, skin, heart wall, urinary bladder wall ( $P < 0.0001$ ), and pituitary gland ( $P = 0.0252$ ). The contributions from remainder of body, source tissues, and target tissue to the total absorbed dose coefficients for kidney and urinary bladder wall are shown in Figure 4.

### DISCUSSION

The main objective of radiopharmaceutical dosimetry for diagnostic agents is to

**TABLE 2**  
Absorbed Dose Coefficients for  $^{68}\text{Ga}$ -DOTATATE (mGy/MBq) in Normal Tissues and Organs

Site	ICRP 110	CE	Sandström et al. (10)	Walker et al. (9)
Spleen	$0.25 \pm 0.097$	$0.28 \pm 0.11$	$0.11 \pm 0.058$	$0.28 \pm 0.12$
Pituitary gland	$0.15 \pm 0.062$	$0.22 \pm 0.092$	—	$0.042 \pm 0.032$
Kidneys	$0.14 \pm 0.048$	$0.15 \pm 0.055$	$0.093 \pm 0.016$	$0.092 \pm 0.028$
Adrenal glands	$0.11 \pm 0.037$	$0.11 \pm 0.041$	$0.086 \pm 0.052$	$0.015 \pm 0.001$
Liver	$0.084 \pm 0.019$	$0.088 \pm 0.022$	$0.050 \pm 0.015$	$0.045 \pm 0.015$
Gallbladder wall	$0.043 \pm 0.008$	$0.015 \pm 0.002$	$0.016 \pm 0.002$	$0.015 \pm 0.001$
Urinary bladder wall	$0.040 \pm 0.011$	$0.090 \pm 0.033$	$0.098 \pm 0.048$	$0.13 \pm 0.062$
Effective dose coefficient (mSv/MBq)	$0.023 \pm 0.003$	$0.027 \pm 0.005$	$0.021 \pm 0.003$	$0.026 \pm 0.003$

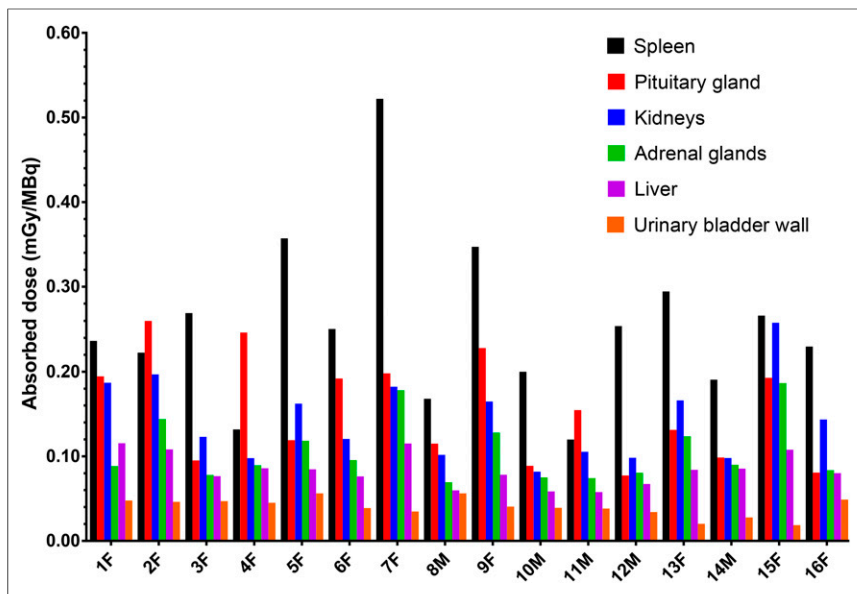


**FIGURE 2.** Absorbed dose coefficients for selected tissues from 16 patients using ICRP 110 phantoms.

ensure that the risks of the imaging procedure are minimal compared with the benefits. Accordingly, dosimetry for diagnostic agents is not performed for any individual patient. Rather, agent-specific pharmacokinetic data from an appropriate patient population are collected and used in conjunction with an internationally recognized standard reference geometry that provides the S values required to perform the calculation. Standardization of all elements required to arrive at an absorbed dose estimate is important in maintaining consistency across centers and ensuring that the values reported in publications reflect actual differences

arising from the properties of the agent rather than from different data acquisition protocols and corresponding S values. The release of a new set of reference geometries and associated tissue-weighting factors requires that physicists and nuclear medicine practitioners transition from the older, CE phantom, set of standards to the newer, ICRP 110 phantom, set. Using data from  $^{68}\text{Ga}$ -DOTATATE, we have investigated the effect on absorbed dose calculations arising from the switch in phantoms and corresponding S values.

In the ICRP 110 phantom-based calculations, the remainder activity was uniformly distributed in the remaining tissues using the respective organ/tissue weights, including blood, according to ICRP 133. The remainder activity in walled organs was uniformly distributed in the wall according to Equation 10 and not in the contents (urinary bladder contents were the exception because urinary bladder was a source region). This explanation accounts to some

extent for the higher absorbed dose coefficients in these walled organs for the ICRP 110 phantoms than for the CE phantoms using the contents as the source. There are also differences in tissues definitions between the ICRP 110 phantoms and the CE phantoms; for example, in the ICRP 110 phantoms, the right colon wall includes the ascending colon wall and the right half of the transverse colon wall, and the left colon wall includes the descending colon wall and the left half of the transverse colon wall. In the CE phantoms, the lower large intestine corresponds to the descending colon, sigmoid colon, and rectum, and the upper

**TABLE 3**  
Average TIACs (h) in Normal Tissues and Organs

Site	Male		Female	
	ICRP 110	CE	ICRP 110	CE
Whole body	1.48E+00 ± 5.67E-02	1.48E+00 ± 5.67E-02	1.48E+00 ± 9.77E-02	1.48E+00 ± 9.77E-02
Remainder of body	4.98E-01 ± 8.01E-02	6.49E-01 ± 6.28E-02	5.17E-01 ± 6.95E-02	6.01E-01 ± 7.63E-02
Muscle	3.17E-01 ± 8.14E-02	2.95E-01 ± 7.58E-02	2.11E-01 ± 7.34E-02	2.29E-01 ± 5.23E-02
Liver	2.90E-01 ± 4.89E-02	2.32E-01 ± 3.92E-02	3.18E-01 ± 5.48E-02	2.59E-01 ± 4.47E-02
Kidneys	8.56E-02 ± 7.97E-03	6.00E-02 ± 5.59E-03	1.25E-01 ± 3.35E-02	1.01E-01 ± 2.72E-02
Spleen	9.54E-02 ± 2.32E-02	7.59E-02 ± 1.84E-02	1.22E-01 ± 4.20E-02	1.03E-01 ± 3.55E-02
Lungs	6.78E-02 ± 1.39E-02	5.60E-02 ± 1.15E-02	5.98E-02 ± 1.97E-02	5.31E-02 ± 1.75E-02
Urinary bladder contents	6.07E-02 ± 1.92E-02	6.07E-02 ± 1.92E-02	5.76E-02 ± 2.16E-02	5.76E-02 ± 2.16E-02
Red marrow	4.47E-02 ± 2.41E-02	3.56E-02 ± 1.92E-02	4.59E-02 ± 2.36E-02	5.91E-02 ± 3.03E-02
Heart wall	8.59E-03 ± 1.54E-03	6.97E-03 ± 1.25E-03	7.48E-03 ± 1.83E-03	6.50E-03 ± 1.59E-03
Salivary glands	3.39E-03 ± 9.17E-04	—	4.87E-03 ± 1.91E-03	—
Brain	4.26E-03 ± 5.30E-04	3.95E-03 ± 4.91E-04	6.10E-03 ± 1.36E-03	5.72E-03 ± 1.27E-03
Adrenal glands	2.91E-03 ± 3.55E-04	2.72E-03 ± 3.32E-04	3.88E-03 ± 1.41E-03	3.69E-03 ± 1.34E-03
Testes	7.60E-04 ± 1.07E-04	7.91E-04 ± 1.11E-04	—	—
Thyroid	6.86E-04 ± 3.10E-04	6.01E-04 ± 2.72E-04	4.64E-04 ± 1.68E-04	4.26E-04 ± 1.54E-04
Pituitary gland	2.71E-04 ± 6.96E-05	2.68E-04 ± 6.90E-05	4.49E-04 ± 1.49E-04	4.73E-04 ± 1.58E-04

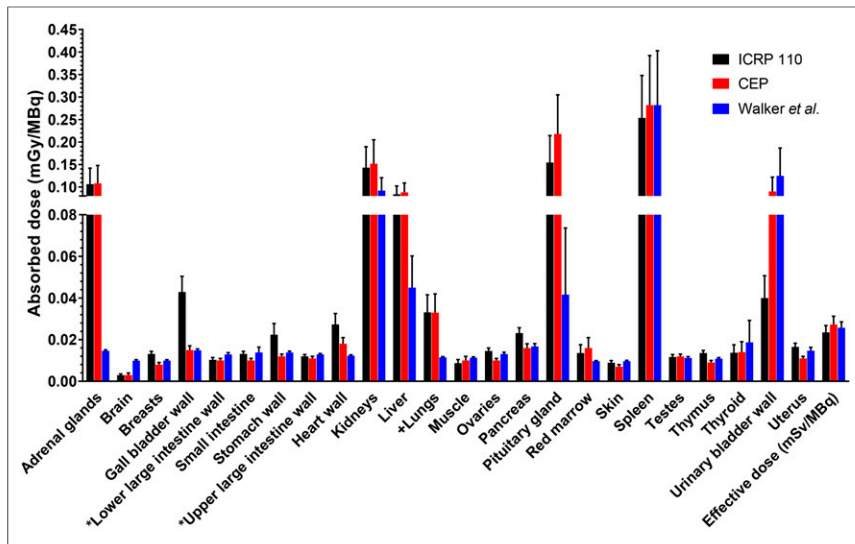


**FIGURE 3.** Comparison of absorbed dose coefficients for ICRP 110 phantoms, CE phantoms (CEP), and previously published results by Walker et al. (9) using OLINDA/EXM, version 1. Error bars = SD. \*Anatomic definition differs between ICRP 110 and CE phantoms. †ICRP 110 phantoms show alveolar-interstitial absorbed dose coefficient, compared with total lung for CE phantoms.

large intestine corresponds to the ascending colon and transverse colon (16). In addition, the lungs are divided into 4 target regions in the ICRP 110 phantoms, compared with 1 target region in the CE phantoms.

When the calculated self-dose S values were compared between the CE and ICRP 110 phantoms, the CE phantom values were higher for both females (range,  $-7.7\%$  to  $+65.3\%$ ) and males (range,  $-961\%$  to  $+59.6\%$ ), with the largest difference being for the urinary bladder contents to the urinary bladder wall ( $+65.3\%$  in females and  $+59.6\%$  in males) and an outlier for the self-dose breast S value ( $-961\%$ ) in males. The standard mass for the male breast was 351 g (11,12) and 26.2 g (6) for the CE and ICRP 110 phantoms, respectively, and is probably the main explanation for the large difference observed in the respective S values. A comparison of the CE and the ICRP 110 phantoms using the averaged male and female self-dose S values for all organs and tissues gave a difference of  $+26.3\%$  and  $+27.1\%$ , respectively, with a respective tissue mass difference of  $-2.2\%$  and  $-6.7\%$ . However, a comparison using the specific TIACs and organ/tissue masses from the ICRP 110 method in the CE method and comparing with the CE phantom results gave an averaged male and female absorbed dose difference of 2.1% for the urinary bladder wall and 1.8% for the kidneys; thus, the effect of mass differences on the results is small because of the scaling of input activity to the phantom organ mass.

In general, the results showed lower absorbed doses using ICRP 110 phantoms than using CE phantoms. This finding is likely explained by 2 fundamental differences between these phantoms. The first is a difference in organ topology, with the ICRP 110 phantoms having less interorgan tissue space and a better accounting and placement of distributed tissue (e.g., marrow, adipose tissue, and muscle). The second difference is that S values derived from the ICRP 110 phantoms have a better handling of the fraction of electron energy absorbed. This characteristic explains to some extent the larger differences seen in thin-walled organs (e.g., urinary bladder wall, which had a 125% higher absorbed dose

coefficient in the CE phantom calculations than in the ICRP 110 phantom calculations). This advantage leads to a different and better approach to handling TIACs not specifically assigned to source organs. It is now possible to deposit TIACs uniformly throughout the remaining non-source tissue and then use specific source-to-target S values to account for the absorbed dose due to a TIAC that is not specifically allocated. Other differences in the calculations (e.g., updated radionuclide decay data (17) and tissue densities) had negligible effects on the differences, as previously shown by Hadid et al. (18).

Dosimetric calculations for  $^{68}\text{Ga}$ -DOTA-TATE have previously been published by Walker et al. (9) and Sandström et al. (10). The percentage difference between results obtained in this study using the CE phantoms and those of Walker et al. ranged from  $-229\%$  to  $+86.5\%$  (brain and adrenal glands, respectively). The absorbed dose coefficient to the adrenal glands reported by Sandström et al. was 21% lower than that

obtained in this study. The large adrenal-gland difference for Walker et al. could be explained by their not using the adrenal glands as a source organ (no contour was drawn), whereas our study and that of Sandström et al. did use drawn contours. In addition, the absorbed dose coefficient to the salivary glands calculated by Walker et al. ( $0.012 \pm 0.008$  mGy/MBq) was 52% lower than that obtained using the ICRP 110 phantom calculation ( $0.025 \pm 0.010$  mGy/MBq). Similarly, the salivary glands were not included in the CE phantoms as a source or target region. In addition, Walker et al. used data exclusively from male patients, whereas our study used the average between male and female. For both the salivary and the pituitary glands, there were significant differences ( $P < 0.035$ ) between the male and female absorbed dose coefficients (Fig. 1). In addition, because the ICRP 110 phantoms use the salivary glands both as a source and as a target region, the absorbed dose considers not only the self-dose but also contributions from adjacent and surrounding tissues (unlike version 1 of the OLINDA/EXM sphere model, for example). Furthermore, Walker et al. did not perform whole-body PET/CT and made estimates for the activity in the nonimaged extremities to get the whole-body activity. Sandström et al. also did not perform whole-body PET/CT but, rather, scanned from the base of the skull to the proximal femur. Because we performed whole-body (head to toes) scans in this work, we were able to account for all the activity in the body.

Figure 4 depicts the averaged male and female contribution from different source tissues to the kidneys and urinary bladder wall. These 2 tissues were chosen to illustrate the differences in relative contribution to the total absorbed dose between a solid organ and a walled tissue, respectively. As expected, self-dose is the dominant contributor to the total absorbed dose for the kidneys. In contrast, urinary bladder contents provide a greater contribution to the bladder wall dose than does the wall itself, as can be seen in the ICRP 110 bladder wall dose calculation. Urinary bladder wall self-dose S values are available for the ICRP 110 phantom calculations but not for the CE phantom calculations. The absorbed dose coefficient for the kidneys was 5.9% higher

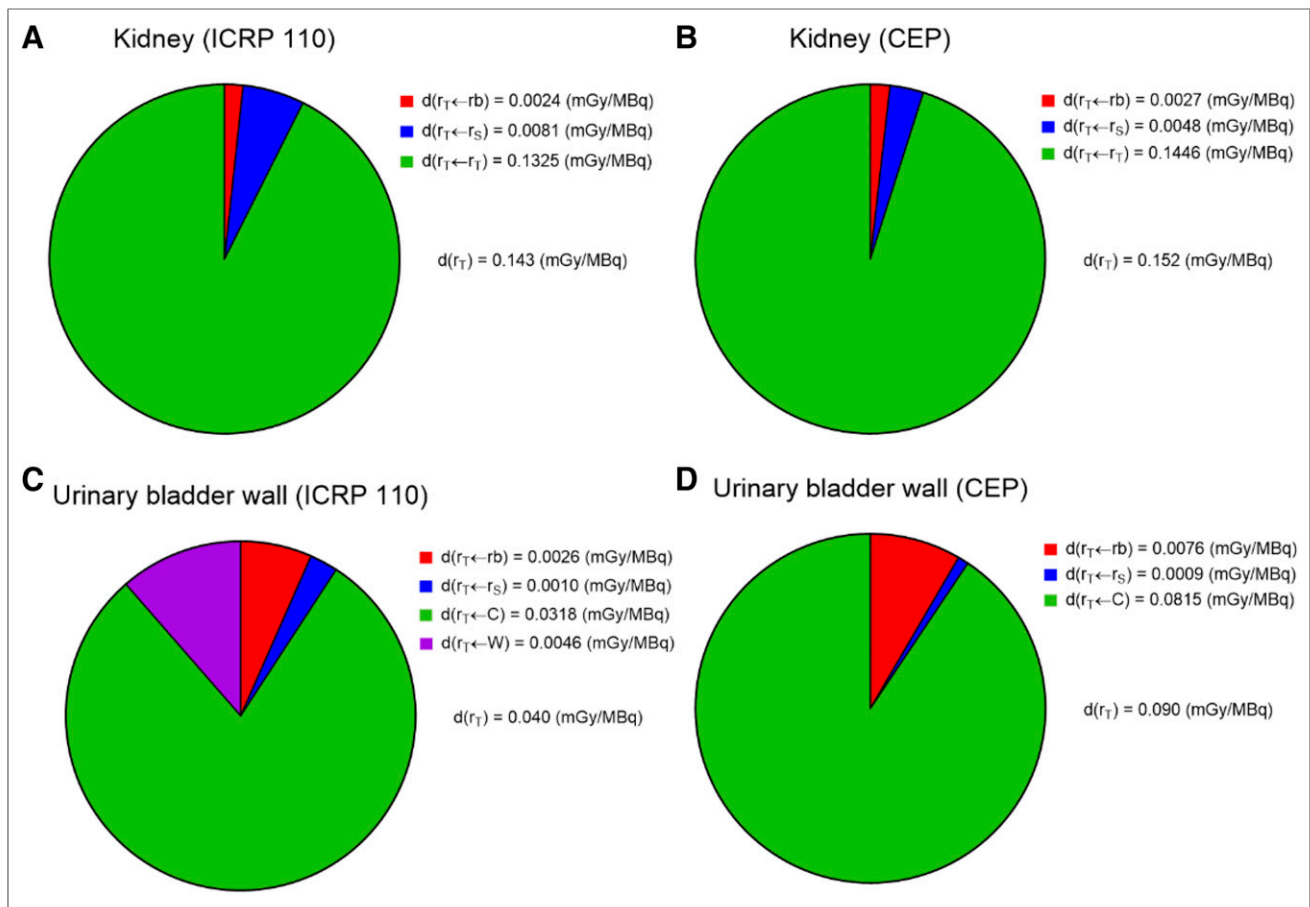


**FIGURE 4.** Contribution from target region, source region, and remainder of body to total absorbed dose coefficient in target regions ICRP 110 kidney (A), CE kidney (B), ICRP 110 urinary bladder wall (with contribution from contents and wall) (C), and CE urinary bladder wall (with contribution from contents) (D). CEP = CE phantoms.

for the CE phantoms than for the ICRP 110 phantoms, as can be explained mainly by a 29.7% higher self-dose  $S$  value, a 30.7% lower average kidney TIAC, and the difference in contributions from source tissues and remainder of body. For the urinary bladder wall, the absorbed dose coefficient was 125% higher for the CE phantoms than for the ICRP 110 phantoms, as can be explained mainly by a 62.5% higher urinary bladder contents-to-wall  $S$  value, no difference in TIAC (the TIACs for urinary bladder contents were calculated using the MIRD bladder-voiding model as implemented in OLINDA/EXM, version 1, and is not phantom-dependent), and the difference in contributions from source tissues and remainder of body (including urinary bladder wall for the ICRP 110 phantoms). This difference stems from a difference in methods, with the CE phantoms using only contents as a source for walled organs (e.g., stomach, gallbladder, intestine, and urinary bladder) but the ICRP 110 phantoms using organ wall as a source as well.

As shown in Figures 2 and 3, the calculated absorbed dose coefficients for the different organs/tissues varied widely among patients, with the differences being in many cases larger than those between the ICRP 110 and CE phantom calculations. About half the compared organs/tissues (mainly those that are small or walled) differed significantly between the ICRP 110 and CE phantom calculations. The calculated absorbed doses for larger solid organs (e.g., liver) did not significantly differ between the ICRP

110 and CE phantoms. The significant differences in the smaller or walled organs represent relatively low absorbed doses compared with larger solid organs such as the spleen. Tissue-absorbed doses are already low for diagnostic agents. The modest reduction in tissue-absorbed doses and in effective dose will have a minimal impact on routine clinical practice. The main impact of these updated calculations will be in the development of new imaging agents. In this context, lower absorbed doses would allow slightly greater administered activities and therefore higher-quality images.

Another area that would be impacted, although negatively so, is the therapeutic use of radionuclides. Even though dosimetry for radiopharmaceutical therapy should account for individual patient anatomy and the spatial distribution of activity within organs, standard phantom-based dosimetry methods are still used for initial assessments of likely toxicity and for reporting to regulatory authorities.

The tissue-weighting factors used with the ICRP 110 phantoms were from ICRP 103, whereas those used with the CE phantoms were from ICRP 60. The main change from the earlier tissue-weighting factors is a decrease for gonads, an increase for breast, the use of separate weighting factors for salivary glands and brain, and an increase for the remainder category, both in value and in number of tissues included (7,8). The calculated effective dose coefficient was significantly lower for the ICRP 110 phantoms than for the CE phantoms. The recommended administered activity of  $^{68}\text{Ga}$ -DOTATATE (range, 100–200 MBq) (19)—and the

average administered in this study—was 131.2 MBq. According to the ICRP 110 phantoms, this amount of activity results in an effective dose of 3.0 mSv (2.3–4.6 mSv for the recommended activity range), which is lower than the 3.6 mSv calculated using the CE phantoms. Accordingly, effective doses have been overestimated using the CE phantoms, as compared with the ICRP 110 phantoms in combination with specific absorbed fractions from ICRP 133 and tissue-weighting factors from ICRP 103.

## CONCLUSION

CE phantom-based dosimetry has been shown to overestimate effective dose. The differences that were found between CE phantom-based dosimetry and ICRP 110-based dosimetry for  $^{68}\text{Ga}$ -DOTATATE may require a reevaluation of the dosimetry for other diagnostic agents as well. These new standards should be adopted rapidly so as to minimize confusion in the dosimetry literature.

## DISCLOSURE

This work was supported by FAPESP 13/03876-4 (“Avaliação do uso do  $^{68}\text{Ga}$ -peptídeo análogo de somatostatina PET/CT como ferramenta diagnóstica em tumores neuroendócrinos e sua correlação com marcadores moleculares”) and by NIH R01 CA116477. No other potential conflict of interest relevant to this article was reported.

## ACKNOWLEDGMENTS

Drs. George Barberio Coura Filho and Ana Amélia Fialho de Oliveira Hoff, from Instituto do Cancer do Estado de São Paulo, are acknowledged for helping us acquire the PET/CT images. We also thank Dr. William Goodwin, from the Department of Biomedical Engineering at the University of Florida, for valuable information and insight on the ICRP 110 voxelized phantoms.

## REFERENCES

1. Loevinger R, Budinger T, Watson E. *MIRD Primer for Absorbed Dose Calculations*. Reston, VA: The Society of Nuclear Medicine and Molecular Imaging; 1991:1–128.
2. Bolch WE, Eckerman KF, Sgouros G, Thomas SR. MIRD pamphlet no. 21: a generalized schema for radiopharmaceutical dosimetry—standardization of nomenclature. *J Nucl Med*. 2009;50:477–484.
3. Cristy M, Eckerman KF. *Specific Absorbed Fractions of Energy at Various Ages from Internal Photon Sources. III. Five-Year-Old*. Oak Ridge, TN: Oak Ridge National Laboratory; 1987:1–42. ORNL/TM-8381/V3.
4. Menzel HG, Clement C, DeLuca P. ICRP publication 110: realistic reference phantoms—an ICRP/ICRU joint effort. A report of adult reference computational phantoms. *Ann ICRP*. 2009;39:1–164.
5. Basic anatomical and physiological data for use in radiological protection: reference values—a report of age- and gender-related differences in the anatomical and physiological characteristics of reference individuals. ICRP publication 89. *Ann ICRP*. 2002;32:5–265.
6. Bolch WE, Jokisch D, Zankl M, et al. The ICRP computational framework for internal dose assessment for reference adults: specific absorbed fractions—ICRP publication 133. *Ann ICRP*. 2016;45:1–74.
7. The 2007 recommendations of the International Commission on Radiological Protection: ICRP publication 103. *Ann ICRP*. 2007;37:1–332.
8. 1990 recommendations of the International Commission on Radiological Protection: ICRP publication 60. *Ann ICRP*. 1990;21:1–227.
9. Walker RC, Smith GT, Liu E, Moore B, Clanton J, Stabin M. Measured human dosimetry of  $^{68}\text{Ga}$ -DOTATATE. *J Nucl Med*. 2013;54:855–860.
10. Sandström M, Velikyan I, Garske-Román U, et al. Comparative biodistribution and radiation dosimetry of  $^{68}\text{Ga}$ -DOTATOC and  $^{68}\text{Ga}$ -DOTATATE in patients with neuroendocrine tumors. *J Nucl Med*. 2013;54:1755–1759.
11. Stabin MG, Sparks RB, Crowe E. OLINDA/EXM: the second-generation personal computer software for internal dose assessment in nuclear medicine. *J Nucl Med*. 2005;46:1023–1027.
12. Stabin MG, Tagesson M, Thomas SR, Ljungberg M, Strand SE. Radiation dosimetry in nuclear medicine. *Appl Radiat Isot*. 1999;50:73–87.
13. Thomas SR, Stabin MG, Chin-Tu C, Samaritunga RC. MIRD pamphlet no. 14 revised: a dynamic urinary bladder model for radiation dose calculations. *J Nucl Med*. 1999;40(suppl):102S–123S.
14. Plyku D, Hobbs RF, Huang K, et al. Recombinant human thyroid-stimulating hormone versus thyroid hormone withdrawal in  $^{124}\text{I}$ -PET/CT based dosimetry for  $^{131}\text{I}$  therapy of metastatic differentiated thyroid cancer. *J Nucl Med*. 2017;58:1146–1154.
15. Coffey JL, Watson EE. Calculating dose from remaining body activity: a comparison of two methods. *Med Phys*. 1979;6:307–308.
16. Snyder WS, Cook MJ, Nasset ES, Karhausen LR, Howells GP, Tipton IH. *Report of the Task Group on Reference Man: ICRP Publication 23*. New York, NY: Pergamon Press; 1975:1–480.
17. Eckerman K, Endo A. ICRP publication 107: nuclear decay data for dosimetric calculations. *Ann ICRP*. 2008;38:1–96.
18. Hadid L, Gardumi A, Desbree A. Evaluation of absorbed and effective doses to patients from radiopharmaceuticals using the ICRP 110 reference computational phantoms and ICRP 103 formulation. *Radiat Prot Dosimetry*. 2013;156:141–159.
19. Virgolini I, Ambrosini V, Bomanji JB, et al. Procedure guidelines for PET/CT tumour imaging with  $^{68}\text{Ga}$ -DOTA-conjugated peptides:  $^{68}\text{Ga}$ -DOTA-TOC,  $^{68}\text{Ga}$ -DOTA-NOC,  $^{68}\text{Ga}$ -DOTA-TATE. *Eur J Nucl Med Mol Imaging*. 2010;37:2004–2010.